Through-Wall Multistatic Polarimetric 3D SAR

Daniel Andre[1], Richard Sabiers[1], Mark Finnis[2]
[1]Centre for Electronic Warfare, Information and Cyber
[2]Centre for Defence Engineering
Cranfield University
Defence Academy of the United Kingdom
UNITED KINGDOM

d.andre@cranfield.ac.uk

ABSTRACT

Through-Wall (TW) Synthetic Aperture Radar (SAR) imagery can be difficult to interpret due to several factors including signal attenuation in highly cluttered environments, target overlay, difficult to interpret low SAR resolution and low frequency scattering responses. One approach which may help improve image interpretability is to employ 2D SAR apertures with multiple distributed receivers in all polarizations. For example: the 2D SAR aperture would allow the formation of 3D images, reducing noise levels and clutter overlay, as well as improving the recognition of objects through providing height information; the distributed receivers would be more likely to capture any bright specular responses from targets in the scene, making them visible; the polarimetric collection may provide useful target information, such as its orientation, polarizability or number of interactions with the radar signal. Highlight results from TW-SAR bistatic polarimetric experiments at the Cranfield University GBSAR laboratory are presented, illustrating the utility of the approach.

1. INTRODUCTION

Through-Wall (TW) Synthetic Aperture Radar (SAR) images can be difficult to interpret due to factors including signal attenuation, highly cluttered environments, target overlay due to the 3D nature of the scene, low SAR resolution and low frequency scattering responses which can be resonant in nature.

An approach which can help improve image interpretability is to employ 2D SAR apertures with multiple distributed receivers in all polarizations. For example, the 2D SAR aperture would allow the formation of 3D SAR images which would reduce noise levels and clutter overlay, as well as improving the recognition of objects through providing height information. If the receivers are distributed about the scene, the multistatic aperture would be more likely to capture any bright specular responses from targets in the scene, making them more visible. A polarimetric collection could provide further useful target information, such as its orientation, polarizability or number of interactions with the radar signal.

This paper presents selected results from TW-SAR bistatic polarimetric experiments performed recently at the Cranfield University GBSAR laboratory, illustrating the utility of the approach. Section 2 describes the bistatic polarimetric decomposition employed in the study; Section 3 discusses the laboratory measurements, describing the laboratory system, some results on canonical scatterers and on a mock building structure. Initial three-dimensional SAR images, both monostatic and bistatic are also presented.

2. BISTATIC POLARIMETRIC DECOMPOSITION

Whilst monostatic polarimetric decompositions are well understood, bistatic generalizations of these are not well-known and the physical interpretation of many of those proposed are not clear. Some of the bistatic decomposition approaches are only slight modifications of existing monostatic approaches, for example

simply introducing an anti-symmetric component to the target scattering matrix (which is always symmetric in the monostatic case). However, the physical meaning associated with this polarimetric parameter extraction may be unclear, and increasingly so where the geometry is far from the monostatic case.

The approach selected for application in this work, is that described by Titin-Schnaider [1-3], constituting a bistatic generalization of the Huynen Fork parameter decomposition [4], providing six polarimetric parameters: for the bistatic case there are two Orientation angles and two Symmetry angles associated with the "incident" and "scattered" ray directions. The formalism has been related to a generalization of the Cloude-Pottier parameters [3].

The bistatic generalization of the Huynen Fork target parameters was found to provide a physically meaningful pixel based polarimetric decomposition [2]. In the monostatic case there are four parameters of interest θ τ ν γ (theta, tau, nu, gamma) representing:

- Orientation / Tilt angle θ is linked to the angle between the projection of the scatterer main axis and the horizontal reference angle:
  - $-90° \leq \theta \leq 90°$. Here we define a positive rotation as clockwise about the down-range direction.
  - Scatterers for which the tilt angle may be meaningful include rods / dipoles and straight edges of extended objects.

- Symmetry angle τ allowing the separation of symmetric and non-symmetric scatterers. A symmetric scatterer is symmetric about a plane containing the incident ray,
  - $0° \leq |\tau| \leq 45°$, where 0° indicates high symmetry, and $|\tau|=45°$ indicates low symmetry,
  - Scatterers with high symmetric would include spheres, rods / dipoles and corner reflectors.

- Skip angle ν divides scatters into two classes according, approximately, to whether the scattered rays have had an odd or even number of radar ray bounces:
  - $0° \leq |\nu| \leq 45°$, where 0° indicates an Odd-bounce interaction and $|\nu|=45°$ indicates an Even-bounce interaction,
    - Odd-bounce scatterers include spheres, flat plates and trihedral multi-bounce. Note that from certain directions, the trihedral response can be dominated by single flat plate, even double-bounce responses or straight edge diffraction.
    - Even-bounce scatterers include dihedral multi-bounce. Note that at certain aspects the dihedral response may be dominated by single flat plate responses or straight edge diffraction.

- Polarizability angle γ, in this approach is taken to mean that the scatterer only returns waves with a particular polarization regardless of incident polarization, hence a polarization projection:
  - $0° \leq \gamma \leq 45°$, where 0° indicates high polarizability and 45° low.
    - Scatterers with medium to high polarizability include rods and the straight edges of extended objects.
    - Scatterers with low polarizability include spheres, flat plates, corner reflectors with multi-bounce including both dihedrals and trihedrals.

For the bistatic case there are two τ parameters, τ_i τ_s, and two θ parameters, θ_i θ_s, – "i" stands for the incident direction, and "s" stands for the scattered direction. In the monostatic case these directions are equivalent, so that the τ values become the same and the θ values too. It is noted that once the orientation parameters are determined (θ_i, θ_s), the additional Huynen parameters provide information intrinsic to the electromagnetic mechanism itself, that is, independent of input and output antenna orientations.

3. LABORATORY MEASUREMENTS

3.1 SAR System

The radar measurements were performed with a vector network analyser, and over the frequency band 1-4 GHz in a space approximately 8m-by-8m in the horizontal and 4m in the vertical, seen in Figure 3-1 left. Initially single polarization wideband microwave horns were used, so that to achieve the four linear polarization combinations these had to be successively rotated for the different scans. In latter experiments dual polarization horns were used, controlled via microwave switches. The horns are seen in a monostatic configuration in Figure 3-1 left, where they are mounted on a scanning system which can move them across an aperture 3.5 m wide and 1.5 m tall, providing a SAR aperture. For the bistatic SAR collections, the receiver horn was placed on a tripod at specific locations about the scene, leaving the transmitter on the scanner (Figure 3-1 right). Combinations of spheres and rods were employed for system calibration [5].

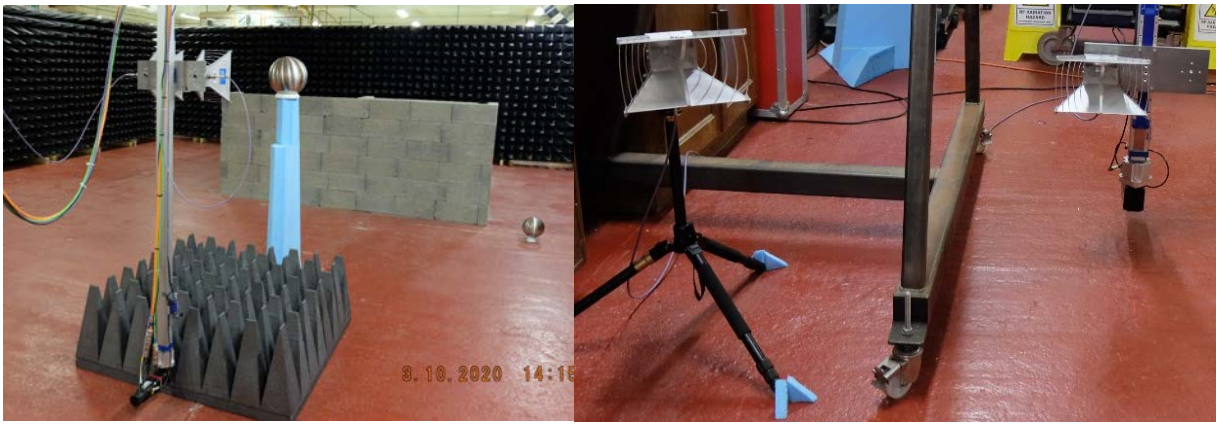

Figure 3 1, Microwave antennas in monostatic configuration undergoing calibration (left), and in bistatic configuration (right).

3.2 Canonical Scatterer Measurements

To test the polarimetric parameter extraction methodology, canonical reflectors were measured including spheres, corner reflectors, cylinders, rods and flat plates. In particular, the dihedral and sphere seen in Figure 3-2 were measured. The dihedral was rotated in steps of 22.5° from -90° to 67.5° clockwise (about down-range direction), effectively spanning all orientations in 22.5° steps, due to the symmetry of the dihedral ($\theta = \theta \pm 180°$).

Sets of quad polarization SAR images were generated for each dihedral orientation, which allowed per-pixel polarimetric parameter extractions, allowing the generation of coloured polarimetric SAR image results. Sets of eight images are presented, one for each dihedral orientation, -90° to 67.5°. The polarimetric SAR images seen in Figure 3-3 show the Skip (ν) parameter extraction, where red is associated with $|\nu|=0°$ or Odd-bounce, and green is associated with $|\nu|=45°$ or Even-bounce. Radar down-range corresponds to the direction up the page. It is noted that the brightness of the images is given by the polarimetric Span $|VV|^2 + |VH|^2 + |HH|^2 + |HV|^2$ in dB, but the colour is given by the extracted parameter angle with association shown in the figure colour bar.

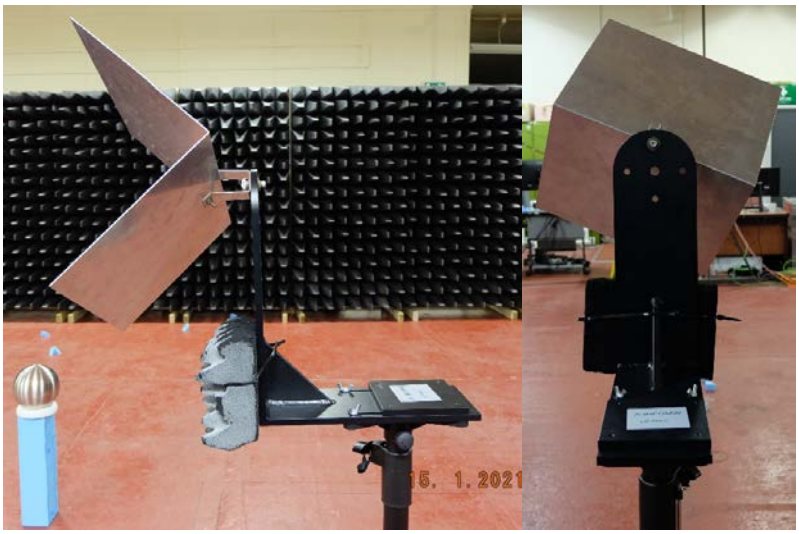

Figure 3-2, Sphere and dihedral targets. The dihedral was rotated to multiple angles.

The triplet of signatures seen on the bottom-left of the images correspond to the raised sphere, where: the closest range signature is the direct sphere interaction and is seen to be Odd-bounce, the next is thought to have a single multipath interaction with the ground and is seen to be Even-bounce, and the third is thought to have had two multipath interactions with the ground and is seen to be Odd-bounce again.

The bright central signature in the images is the main dihedral response. It is seen to be Even-bounce as expected. The width of the signature varies according to the orientation of the dihedral: where the dihedral has a vertical axis orientation, the signature is narrow in cross-range (Figure 3-3, -90° orientation), however where the dihedral has horizontal axis orientation, the signature is wide in cross-range (Figure 3-3, 0° orientation).

It is of interest to note the behaviour of the signatures just up-range from the main dihedral signature. These are the leading-edge dihedral plate signatures, denoted here “DE” (Dihedral Edge), and behave as dipoles / wires. For example, in the vertical orientation image (Figure 3-3, -90° orientation), the leading-edge signatures are two narrow red dots. Indeed, for all the dihedral orientations the DE signatures are strongly Odd-bounce. The width and orientation of the red DE signatures are seen to vary with dihedral orientation as one would expect to see with a plan projection SAR image of the scene.

In Figure 3-4 the polarimetric SAR images showing the Orientation parameter θ_i are presented. The Orientation values for the sphere are recognized as being meaningless, and for the main bright signature of the dihedral they are also unclear. However, for the dihedral plate leading edges “DE” they are meaningful, varying through the Orientation colour association shown on the colour map according to the true orientation of the dihedral. For a quantitative analysis, the polarimetric parameters of the brightest polarimetric Span intensity pixel location within the given feature extent are given in Table 3-1.

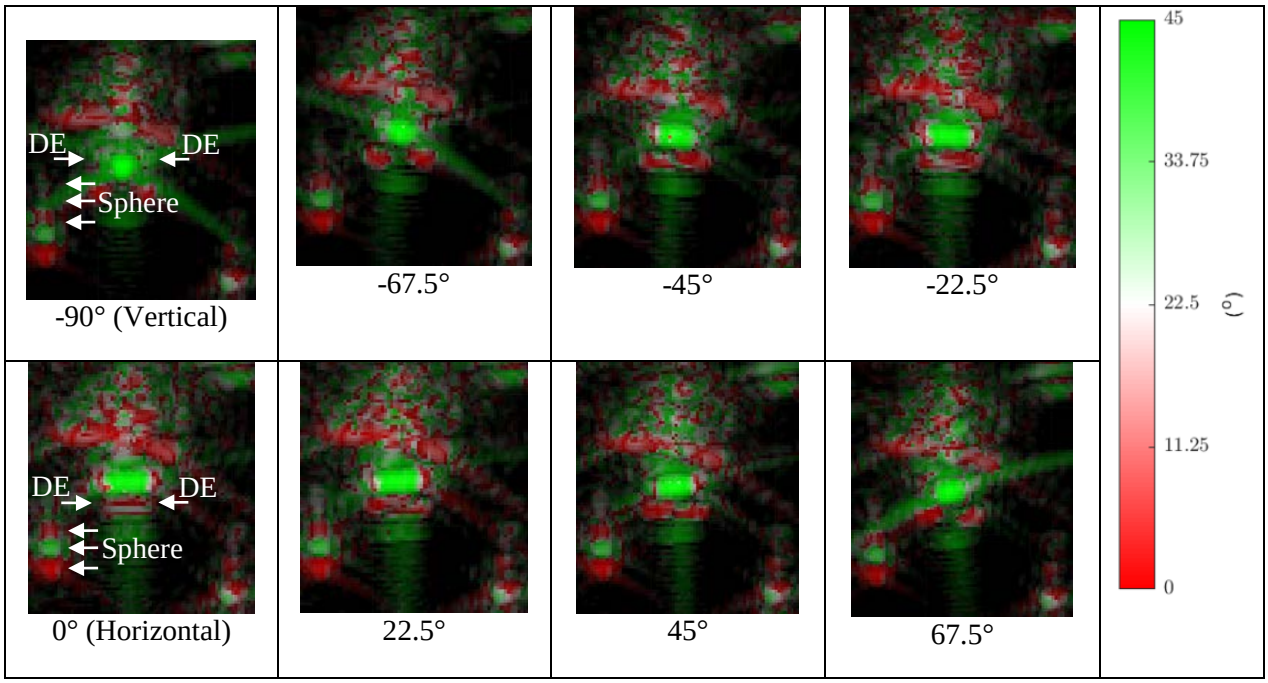

Figure 3-3, Huynen Skip parameter |v| SAR images of the raised sphere and dihedral, showing the variation in signature response as a function of dihedral orientation (angle shown in subplots). The top left image has a vertical dihedral orientation (-90°=90°). The angle of the dihedral increases in 22.5° steps clockwise (about down-range direction) from left to right, and top to bottom. Due to the symmetry of the dihedral, the orientation θ = θ ± 180°.

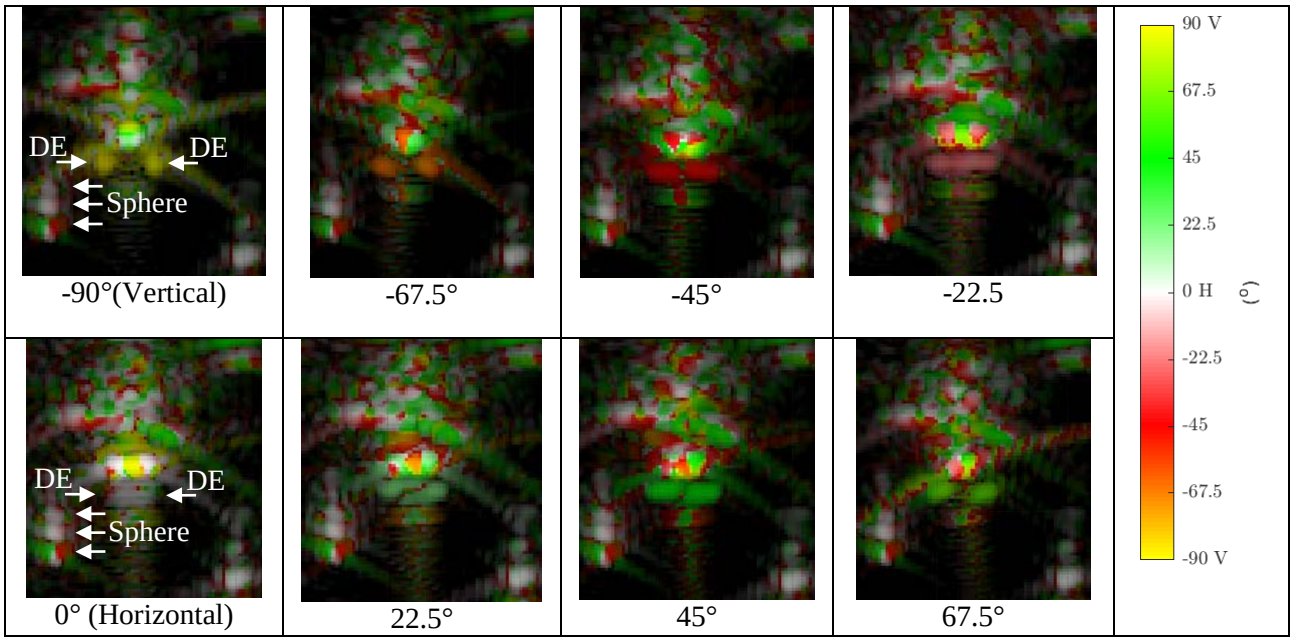

Figure 3-4 Huynen Orientation parameter θi SAR images of the raised sphere and dihedral, showing the variation in responses as a function of dihedral orientation. The top left image has a vertical dihedral orientation (-90°=90°). The angle of the dihedral increases in 22.5° steps clockwise (about down-range direction) from left to right, and top to bottom. Due to the symmetry of the dihedral, the orientation θ = θ ± 180°.

The extracted values for Orientation, θ_i and θ_s, closely match the actual orientations of the dihedral. Generally, the DE signatures can be seen to have low Skip angle $|\nu|$, being Odd-bounce, have high symmetry $|\tau_i|$ $|\tau_s|$, and the polarizabilities γ are seen to have mid-range values.

Table 3-1. Dihedral Edge (DE) Huynen parameter (in °) responses for the different dihedral orientations. The polarimetric parameter values are associated with the brightest polarimetric Span intensity pixel location within the feature extent, and θ = θ ± 180°.

Dihedral angle (°)	θ_i (°)	θ_s (°)	$\|\nu\|$ (°)	$\|\tau_i\|$ (°)	$\|\tau_s\|$ (°)	γ (°)
-90.0	-88.1	-87.8	0.9	1.2	0.7	23.8
-67.5	-66.0	-66.2	1.4	1.0	1.4	20.6
-45.0	-44.6	-44.5	7.9	0.2	0.9	18.2
-22.5	-22.8	-22.6	1.3	0.6	0.9	13.7
0.0	-1.2	0.4	22.8	1.6	1.2	30.0
22.5	19.6	19.4	0.1	1.5	0.4	32.4
45.0	44.5	43.7	1.6	0.2	0.8	30.3
67.5	64.8	64.5	0.3	0.5	1.3	28.3

3.3 Model Building Scene

During the measurement campaign, a model building was constructed, seen in Figure 3-5, approximately 3m-by-3m in size, with a wall height such that there was no radar line of sight into the structure. The main structure was made with concrete bricks and included a partition with doorway, dividing it into two rooms. The right-hand (looking down-range) room leading wall was a cavity wall, whereas the left-hand room walls were single layer brick walls. As well as concrete, the structure had wood and plasterboard panels. Arranged within it were metal cabinets, stools, radiators, electric cables, large metal spheres and diagonally arranged metal pipes. This scene arrangement is denoted MB2ORP (Model Building 2, Office, Radiators, Pipes).

The monostatic (M) Span polarization SAR images can be seen in Figure 3-6 left (the radar points up the page). The radar-facing wall is bright, and the portion with cavity wall has a signature large in range extent. The double layer cavity wall leads to greater attenuation than the single layer wall, and greater target range delay also. Some target signatures are clear, including the sphere and cabinet in the left room, and the radiator, which is up against the back wall.

To distinguish the two metal pipes and two radiator scatterers better, a separate SAR collection was undertaken of the building without these targets in, denoted MB2O. This radar data was coherently subtracted from MB2ORP. The subtraction is shown in Figure 3-6 right. In this image, the two pipes are clearly visible towards the front of the building, denoted P1 and P2 in the image, and the effect of the radiators is visible towards the rear of the building, denoted R1 and R2. For comparison, the radiators and pipes are also designated in the photograph in Figure 3-5. It is noted that as the radiators are up against the rear wall, the visible subtraction signature may be both due to the radiators themselves, and due to a strong subtraction signature involving the shadow they cast on the rear wall. There is an additional feature in the image, denoted PM (Pipe Multipath), thought to be due to multipath between the pipe and the laboratory ceiling. In the corresponding polarimetric parameter extraction for Skip angle ($|\nu|$) in Figure 3-7 top, this signature is seen to be Even-bounce, whereas the pipes and radiators are Odd-bounce. Inspection of the corresponding polarimetric Orientation parameter in Figure 3-7 bottom, shows that the rod orientation has been successfully determined, at about 45°; the orientation of the radiators (R1-2) is indistinct as these are essentially flat plates; the possible multipath signature (MP) is indistinct, possibly due to its low intensity and being subject to clutter.

The SAR scans were repeated for several bistatic geometries also, where receiver locations are fixed. Figure 3-8 shows orientation θ_i coloured Span SAR images, where the receiver is placed on the left of the scene and

on the far left, configurations denoted BL2 and BL3. In the non-subtracted images (Figure 3-8 left) the building corner denoted “BC” is yellow in correspondence with a vertical orientation; and in the subtracted images (Figure 3-8 right) the pipe P1 colour is green, indicating an orientation of approximately 45° (unfortunately an exact laboratory scene ground truth was not obtained for the pipe orientations). Other orientation θ_i signatures are indistinct here, possibly due to a combination of substantial clutter overlay, scatterer type, and the lower resolution attained in the bistatic geometry.

Figure 3-5, model building scene, looking radar up-range (top) and radar down-range (bottom).

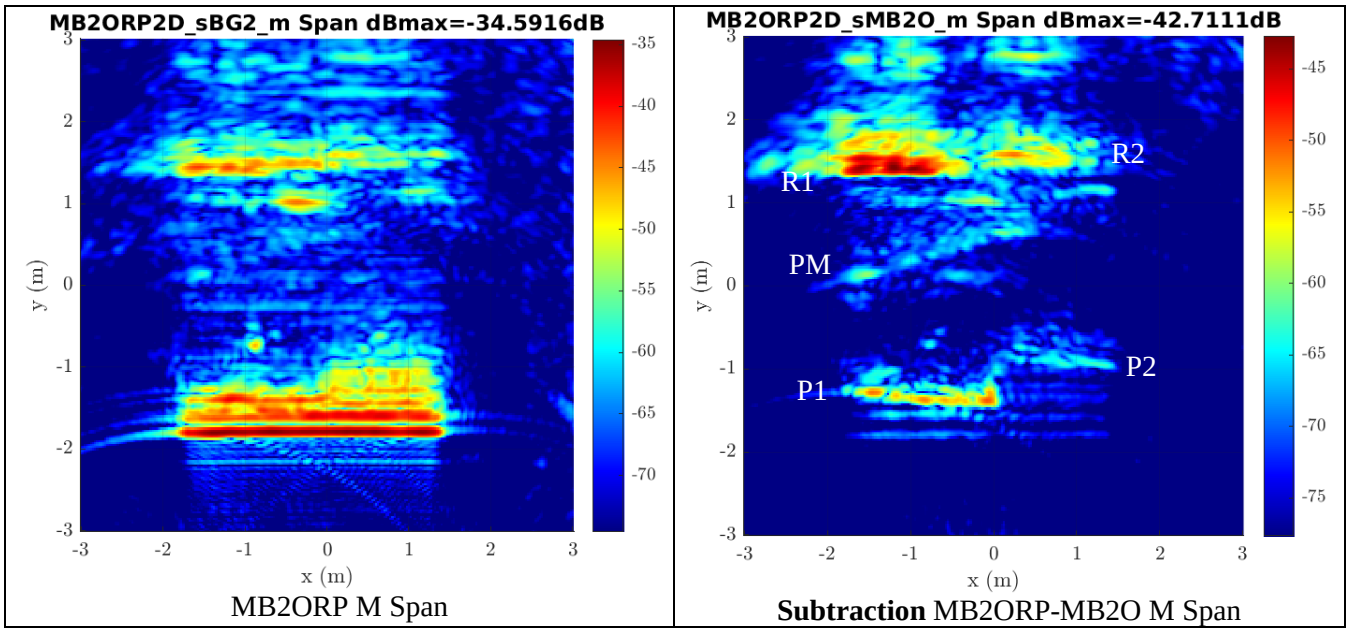

Figure 3-6. polarimetric Span monostatic images of MB2ORP (left) and subtraction MB2ORP-MB2O (right). The pipes (P1, P2) and the radiators (R1, R2) are marked on the subtraction image.

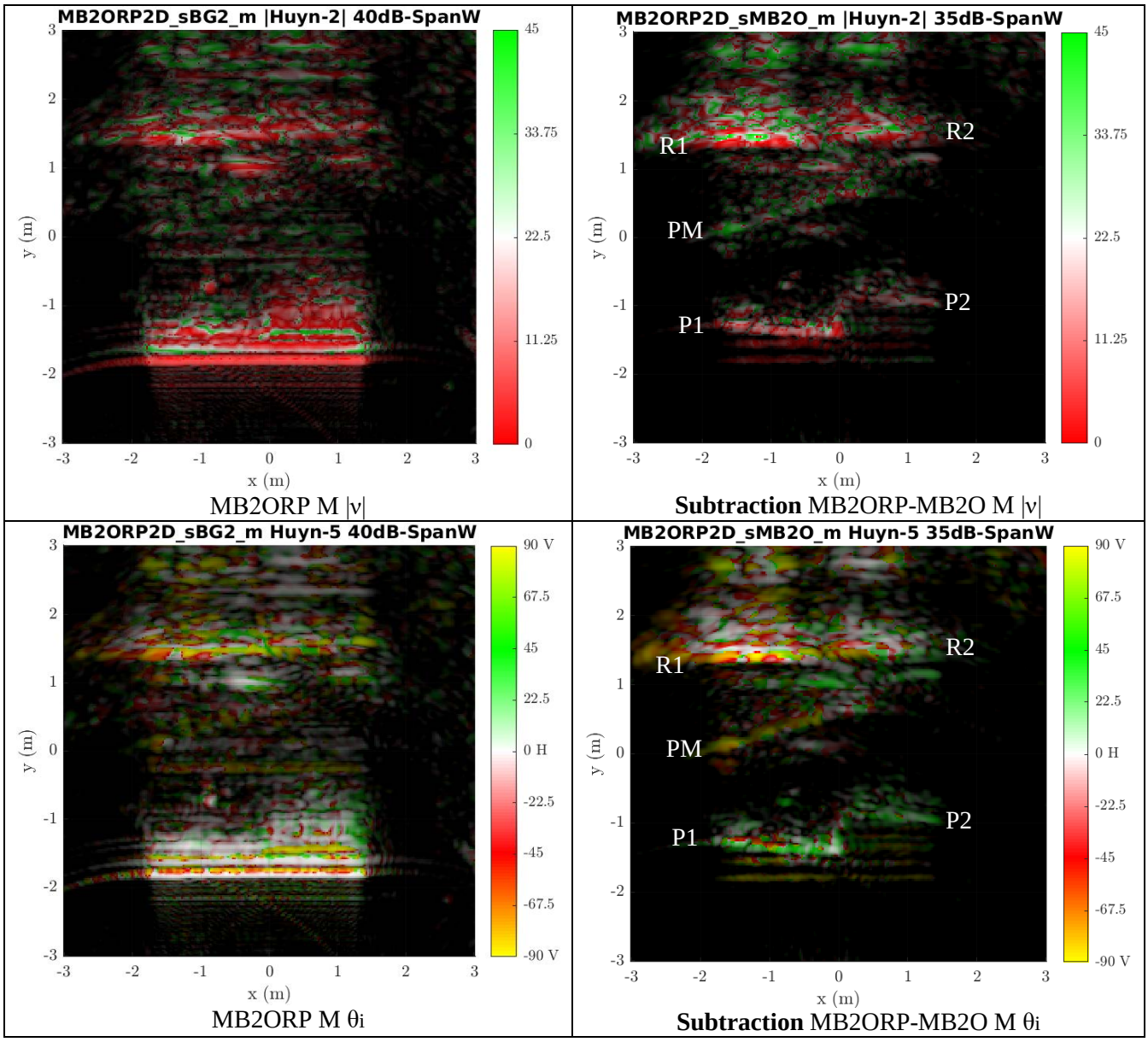

Figure 3-7. Huynen parameter monostatic (M) SAR images of MB2ORP (left) and subtraction MB2ORP-MB2O (right), modulus of Skip (|ν|) (top) and Orientation (θi) (bottom).

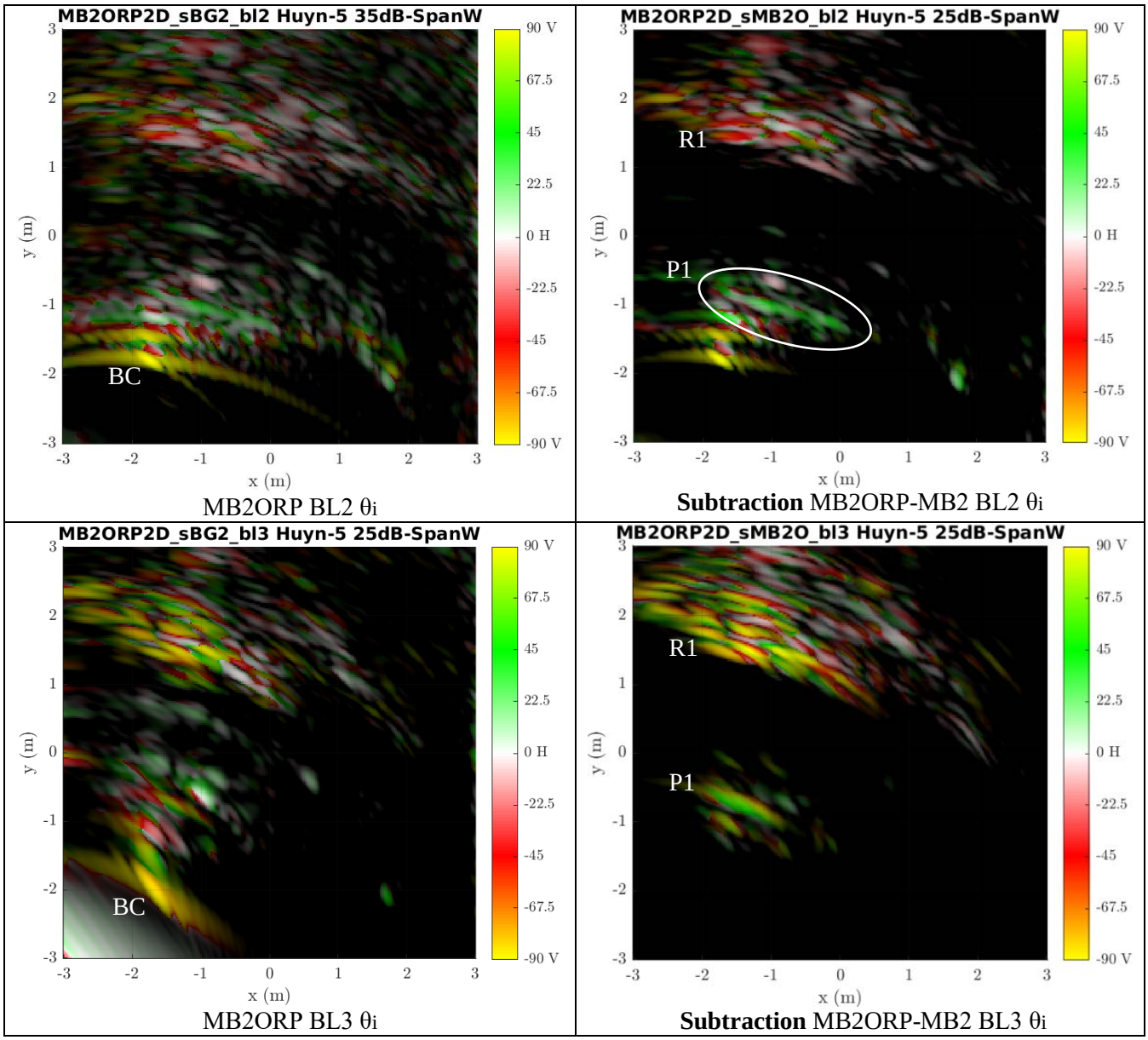

Figure 3-8. Incident Orientation parameter (θi) SAR images, bistatic BL2 (top) and bistatic BL3 (bottom) SAR images of MB2ORP (left) and subtraction MB2ORP-MB2O (right).

3.4 Three-Dimensional SAR Images

To form 3D-SAR images, 2D-SAR apertures were collected in all polarizations. Monostatic results corresponding to those seen for MB2ORP already seen in Figure 3-7, can be seen in Figure 3-9. The coloured renderings were formed with the software Vaa3D [6], with colourmaps equivalent to those used in Figure 3-7.

Figure 3-9 top-left shows a view of the monostatic (M) rendering of the Skip angle, |ν|, weighted by polarimetric Span. The scattering from the leading wall dominates the image and is Odd-bounce (red). Additional scatter details can be seen in the subtraction MB2ORP – MB2O data, which as with the 2D SAR case, reveals the pipes (P1, P2) and the radiators (R1, R2). However, in this case, the actual orientation of the pipe can be seen in the 3D SAR rendering, as well as an indication of the height extent of the radiators. As for the 2D SAR case, here P2 and R2 are dimmer and appear further down-range from their counterparts, due to the double wall with cavity located up-range through which the microwaves have travelled.

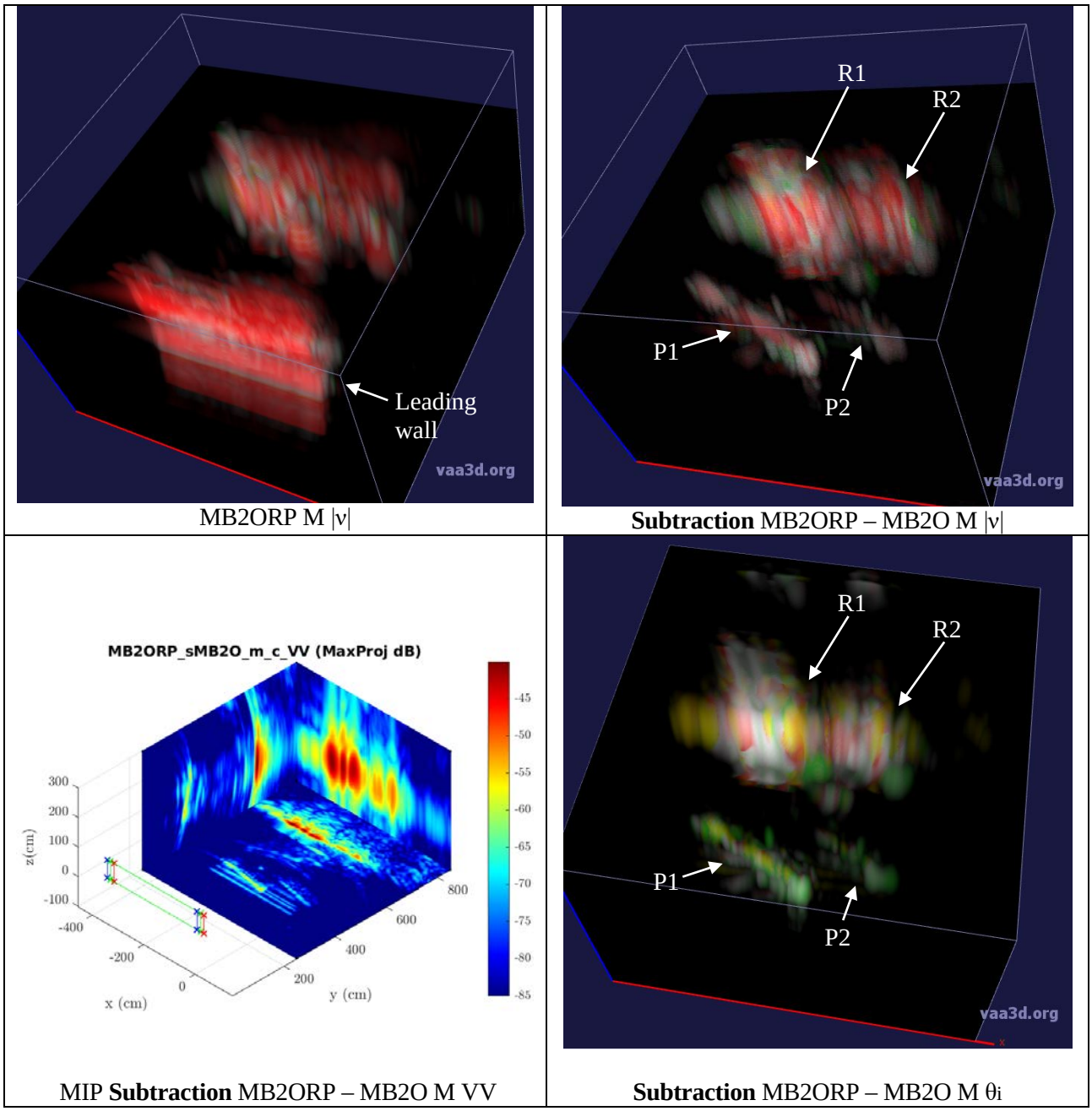

MB2ORP M |ν|

Subtraction MB2ORP – MB2O M |ν|

MIP **Subtraction** MB2ORP – MB2O M VV

Subtraction MB2ORP – MB2O M θi

Figure 3-9. Monostatic 3D SAR images of MB2ORP and subtraction MB2ORP-MB2O data, with volumetric SAR renderings showing both modulus of Skip (|ν|) and Incident Orientation parameter (θi). Maximum intensity 3D SAR projections (MIP) for VV are also presented.

The Orientation θi result is shown in Figure 3-9 bottom-right, showing the pipes in green, indicating an orientation of approximately 45° (unfortunately an exact laboratory scene ground truth was not obtained for the pipe orientations). The Orientation of the radiators is indistinct, as one would expect from a flat plate response.

It is noted that the multipath signature, MP, seen in the 2D SAR image cases in Figure 3-7, is not visible in the 3D SAR images (Figure 3-9). It is thought that this is because the MP signature must be located outside of the 3D SAR focal volume. This is also likely to be the case for other clutter signatures seen in the 2D SAR images.

Maximum intensity projections (MIP) of the VV polarization 3D SAR Subtraction MB2ORP – MB2O image are shown in Figure 3-9 bottom-left. This is a different approach to presenting volumetric image data, where one can see an overview of the volumetric data without the need to rotate it within a viewer. However, information is lost in the projection process, for example the unambiguous orientation of some scatterers, although some orientation information can be regained through polarimetry. It has been found that generally, the 3D renderings (as opposed to the projections) can be rotated and cut in different ways to give more understanding of the volumetric data.

In Figure 3-9 bottom-left, outlines of the 2D SAR rectangular aperture are shown with coloured lines and x's: red for the transmitter aperture, blue for the receiver aperture, and green for the transceiver mid-point aperture.

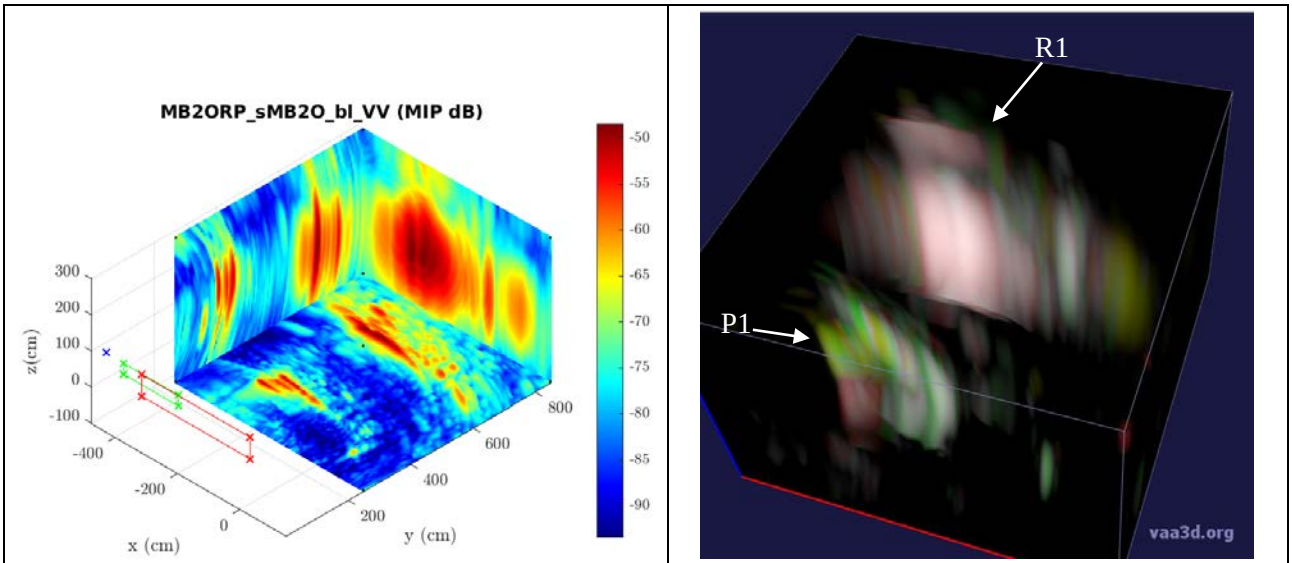

MIP **Subtraction** MB2ORP – MB2O BL VV | **Subtraction** MB2ORP – MB2O BL θ_i

Figure 3-10. Bistatic 3D SAR images of subtraction MB2ORP-MB2O data, with Maximum intensity 3D SAR projections (MIP) for VV (left), and a volumetric SAR rendering showing the Incident Orientation parameter (θ_i) (right).

Bistatic volumetric SAR results are shown in Figure 3-10, for the data subtraction MB2ORP – MB2O. Figure 3-10 left shows maximum intensity projections of the VV polarization image, and the SAR geometry can be seen from the outlines of the 2D SAR aperture, shown with coloured lines and x's: red for the transmitter aperture, a blue "x" for the fixed receiver position, and green for the transceiver mid-point aperture. A volumetric SAR rendering shown with the Orientation θ_i parameter colouring can be seen on the right of the figure.

Due to the fixed receiver positioning, the vertical and horizontal cross-range SAR resolutions are reduced by half, leading to a reduction in image interpretability. It is noted that only the left pipe, P1, and radiator, R1, are visible, but not their counterparts. This is due to the SAR near-field geometry, and to the available specular scattering events on the targets from transmitter to receiver. Due to the poor resolution, the angle of the pipe was not as clearly visible in the bistatic volumetric images, although the orientation signature seems predominately green. When the receiver antenna was placed to the right of the scene, the P2 and R2 scatterers became visible in SAR imagery.

4. CONCLUSION

Selected results from a through-wall monostatic and bistatic polarimetric SAR investigation were presented,

from the GBSAR laboratory at Cranfield University. The system allows 2D bistatic SAR apertures to be collected in quad-polarization over wide frequency bands, of the 8m-by-8m space.

Target scenes consisting of canonical scatterers allowed the evaluation of a bistatic generalisation of a polarimetric Huynen parameter extraction algorithm. A through-wall scenario was also investigated, with a target scene consisting of a mock concrete building with a variety of items inside. Radar data subtraction results showed that change detection can be a useful tool for gaining intelligence of the indoor scene.

Polarimetric parameters provided useful target information, including scatterer orientation and multipath type. This polarimetric information was added to both 2D and 3D SAR images with colouring. 3D SAR images allowed the orientation of scatterers to be confirmed, as well as their position and extent in height. Some clutter and multipath artefacts which were overlayed on 2D SAR images, were not visible in corresponding 3D SAR images, as those features must have been located outside of the 3D SAR focal volume, which can be deemed beneficial for scene understanding.

The bistatic geometries involved a fixed receiver location, which had the effect of reducing both height and azimuth cross-range resolutions. To compensate for this, it would be beneficial to either consider a bistatic aperture with moving receiver antenna, or a multistatic arrangement, involving several fixed receiver antennas, allowing a coherent addition of radar data, providing finer overall cross-range resolutions. The analysis of the three-dimensional multistatic and polarimetric data is ongoing, and laboratory receiver SAR scanner upgrades are being installed.

ACKNOWLEDGMENT

This research was funded by Dstl.

REFERENCES

[1] C. Titin-Schnaider, “Polarimetric Characterization of Bistatic Coherent Mechanisms”, IEEE Transactions on Geoscience and Remote Sensing, Vol.46, No.5, May 2008

[2] C. Titin-Schnaider, “Physical Meaning of Bistatic Polarimetric Parameters”, IEEE Transactions on Geoscience and Remote Sensing, Vol.48, No.5, May 2010

[3] C. Titin-Schnaider, “Characterization and Recognition of Bistatic Polarimetric Mechanisms”, IEEE Transactions on Geoscience and Remote Sensing, Vol.51, No.3, March 2013

[4] J. R. Huynen, “Phenomenological Theory of Radar Targets”, PhD Thesis, TU Delft, 1970

[5] K. Sarabandi, F. Ulaby, M. Tassoudji, “Calibration of Polarimetric Radar Systems with Good Polarization Isolation”, IEEE Transactions on Geoscience and Remote Sensing, Vol.28, No.1, January 1990

[6] Peng, H., Ruan, Z., Long, F., Simpson, J.H., and Myers, E.W. (2010) "V3D enables real-time 3D visualization and quantitative analysis of large-scale biological image data sets," Nature Biotechnology, Vol. 28, No. 4, pp.348-353. (http://vaa3d.org)